INSTITUTE OF PHYSICS PUBLISHING and INTERNATIONAL ATOMIC ENERGY AGENCY NUCLEAR FUSION

Nucl. Fusion **45** (2005) 360–367 doi:10.1088/0029-5515/45/5/006

Effect of ambipolar plasma flow on the penetration of resonant magnetic perturbations in a quasi-axisymmetric stellarator

A. Reiman[1], M. Zarnstorff[1], D. Mikkelsen[1], L. Owen[2], H. Mynick[1], S. Hudson[1] and D. Monticello[1]

[1] Princeton Plasma Physics Laboratory, Princeton, NJ 08543, USA
[2] Oak Ridge National Laboratory, Oak Ridge, TN, USA

E-mail: reiman@pppl.gov

Received 13 December 2004, accepted for publication 3 March 2005
Published 27 April 2005
Online at stacks.iop.org/NF/45/360

Abstract
A reference equilibrium for the US National Compact Stellarator Experiment is predicted to be sufficiently close to quasi-symmetry to allow the plasma to flow in the toroidal direction with little viscous damping, yet to have sufficiently large deviations from quasi-symmetry that nonambipolarity significantly affects the physics of the shielding of resonant magnetic perturbations by plasma flow. The unperturbed velocity profile is modified by the presence of an ambipolar potential, which produces a broad velocity profile. In the presence of a resonant magnetic field perturbation, nonambipolar transport produces a radial current, and the resulting $\boldsymbol{j} \times \boldsymbol{B}$ force resists departures from the ambipolar velocity and enhances the shielding.

PACS numbers: 52.55.Hc, 52.35.Vd, 52.30.-q

1. Introduction

Resonant magnetic perturbations pose a threat to flux surface integrity in toroidal magnetic confinement configurations. The width of the island produced by a resonant perturbation scales as the square root of the perturbation amplitude, so that even a relatively small resonant magnetic perturbation at a rational surface can produce a substantial magnetic island. There has therefore been great interest in the role that plasma flow can play in shielding out resonant perturbations at rational surfaces [1, 2]. This effect is believed to play a major role in reducing the vulnerability of present day tokamaks to resonant field errors, and an understanding of the effect will be important for setting field-error tolerances for ITER. The flow-shielding effect has been studied systematically in tokamak experiments where externally imposed magnetic field perturbations have been varied and their penetration threshold determined [3–5].

This paper considers the flow-shielding effect in a quasi-axisymmetric stellarator. Quasi-axisymmetric stellarator configurations have drift trajectories that look like those in an axisymmetric configuration, and they allow undamped toroidal flow [6]. In the limit of perfect quasi-axisymmetry, the flow-shielding effect is predicted to look like that in a tokamak having the same parameters. However, if we allow for the presence of non-quasi-symmetric ripple in the field, the radial transport is no longer intrinsically ambipolar, as it is in axisymmetric configurations. This brings in an additional radial current which modifies the physics of the flow shielding. The radial current produces a $\boldsymbol{j} \times \boldsymbol{B}$ torque that resists externally induced changes in the flow velocity and enhances the effectiveness of the shielding. It also modifies the unperturbed rotation velocity of the plasma in the absence of a resonant perturbation. Our modelling of these effects employs a one-dimensional transport code [7], as well as the DEGAS code for estimating the momentum transfer rate to neutrals, and the PIES code [8] for calculating the magnitude of the resonant perturbation.

The work described in this paper focuses on a particularly interesting regime of intermediate ripple amplitude, where the deviations from quasi-symmetry are sufficiently large to substantially modify the flow-shielding effect, but where the configuration is nonetheless sufficiently close to quasi-symmetry that the flow damping in the toroidal direction can be considered to be negligibly small compared to that in the poloidal direction. A reference equilibrium for the US National Compact Stellarator Experiment (NCSX) is calculated to be in this intermediate regime, and the numerical

calculations presented in this paper focus on that NCSX reference equilibrium.

The three-dimensional NCSX device will have great flexibility for controlling resonant magnetic field components and investigating their interaction with plasma flow. Comparison of theoretical predictions with experimental observations on NCSX, and with tokamak experiments having comparable plasma parameters, will contribute towards the goal of being able to reliably predict field-error penetration thresholds.

The NCSX, under construction at Princeton, is a quasi-axisymmetric stellarator designed to combine favourable features of advanced tokamaks with those of drift-optimized stellarators [9–11]. The NCSX configuration has been designed to have nested flux surfaces, incorporating several layers of defense against excessive magnetic island formation, but flow shielding could nonetheless have an impact on flexibility and on vulnerability to field errors. The choice of the NCSX fixed boundary configuration was driven, in part, by calculations with the PIES code indicating that it has intrinsically nested flux surfaces [9, 12]. For the design of the NCSX coils to produce this configuration, an optimization code built around the PIES three-dimensional equilibrium code was used to reduce the magnitude of resonant components of the magnetic field while preserving desired engineering and physics properties [12–15]. A series of calculations with the PIES code showed that this coil design process, which targeted the resonant components of the magnetic field in the NCSX reference equilibrium, also greatly reduced the island widths for a range of equilibria with varying profiles, betas and coil currents [12, 16]. The NCSX design also incorporates two sets of trim coils to provide further control over resonant magnetic fields. NCSX has also been designed to have a monotonically increasing $\iota(=1/q)$ profile to give neoclassical suppression of magnetic islands, and this is expected to further protect against magnetic island formation. Nevertheless, to the extent that the plasma flow shields out residual resonant magnetic field components at rational surfaces, it will further improve the flexibility of the NCSX device to generate a range of configurations with nested flux surfaces, and it will further reduce the vulnerability of the NCSX device to field errors produced by finite tolerances in the construction and placement of the magnetic field coils.

Section 2 of this paper will provide an introduction to the physics issues in the shielding of resonant magnetic perturbations by plasma flow in a quasi-axisymmetric stellarator. The remaining sections will discuss the details. The calculations described in this paper have been done for a reference $\beta = 4\%$ NCSX equilibrium whose properties are extensively discussed in a special volume of the journal *Fusion Science and Technology* devoted to the NCSX physics design [17]. Figure 1 shows the shape of the plasma boundary at several poloidal cross sections separated by $\Delta\phi = \pi/9$. (NCSX is a three-period stellarator.) Figure 2 shows the $\iota = 1/q$ (rotational transform) profile plotted as a function of the toroidal flux normalized to its value at the plasma boundary. (Note that some authors use iota-bar rather than iota to denote $1/q$.)

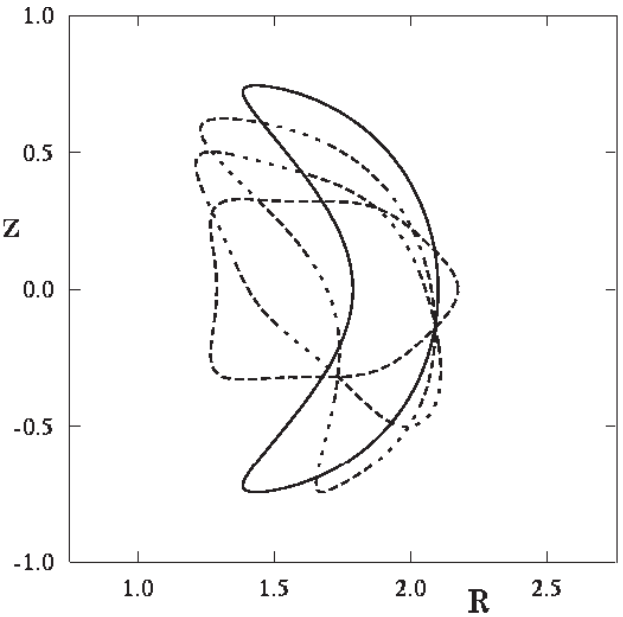

Figure 1. Plasma boundary shape of reference quasi-axisymmetric configuration at poloidal cross sections separated by $\Delta\phi = \pi/9$.

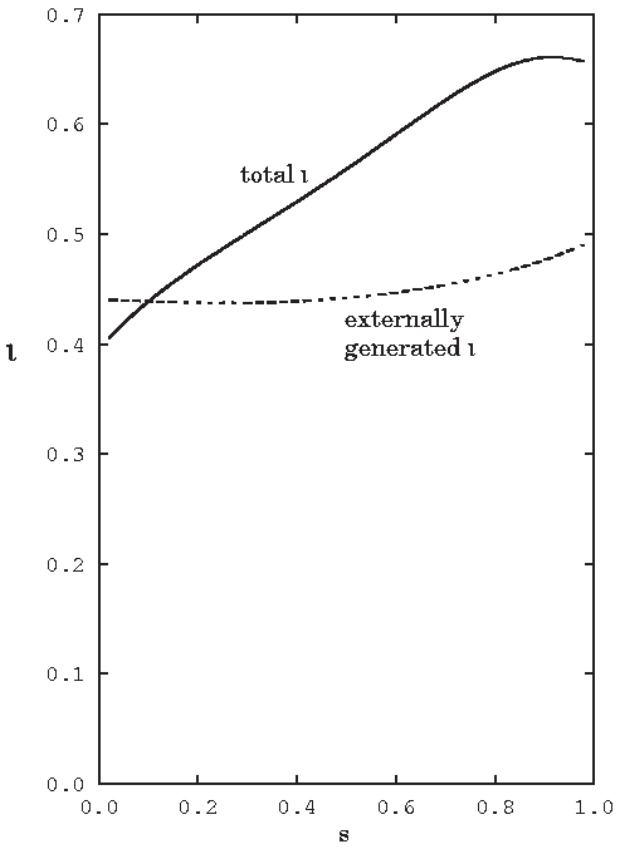

Figure 2. Plot of rotational transform profile, $\iota = 1/q$, as a function of toroidal flux normalized to its value at the plasma boundary.

2. Shielding of rational surfaces by plasma flow in a quasi-axisymmetric stellarator

In an ideal plasma, reconnection is prohibited and the flux surfaces cannot be broken. A surface current is induced

at the rational surface that shields out resonant magnetic perturbations. In the absence of plasma flow, the presence of even a small resistivity causes the surface current to decay, and allows the resonant field to penetrate the rational surface. If flow is present at the rational surface, a localized current continues to be induced which partially shields out the resonant component of the field. (The physics of this is perhaps seen more clearly in a reference frame moving with the plasma, where the resonant perturbation is time dependent.) If the flow is sufficiently strong, only a very small fraction of the resonant field penetrates the rational surface.

The induced current at the rational surface interacts with the remnant of the resonant field there to produce a $\boldsymbol{j} \times \boldsymbol{B}$ torque. This electromagnetic torque opposes the motion of the plasma at the rational surface, and acts to slow the flow. When the resonant perturbation amplitude exceeds a threshold value, the torque is large enough to locally suppress the plasma flow, allowing the resonant perturbation to fully penetrate the rational surface.

Consider the case where a small perturbation of the magnetic field is turned on in a stellarator plasma that initially has nested flux surfaces. Express the unperturbed magnetic field in magnetic coordinates: $\boldsymbol{B}_0 = \nabla\Psi_0 \times \nabla\theta + \iota\nabla\Psi_0 \times \nabla\varphi$, where $\boldsymbol{B}_0$ is the unperturbed field, and Ψ_0 is an unperturbed flux function satisfying $\boldsymbol{B}_0\cdot\nabla\Psi_0 = 0$. Write $\boldsymbol{B} = \boldsymbol{B}_0 + \boldsymbol{\delta B}$, $\Psi = \Psi_0 + \delta\Psi$. To first order $\boldsymbol{B}_0\cdot\nabla(\delta\Psi) = -\boldsymbol{\delta B}\cdot\nabla\Psi_0$. In magnetic coordinates this can be expressed as

$$\boldsymbol{B}_0\cdot\nabla\varphi\left(\frac{\partial\delta\Psi}{\partial\varphi} + \iota\frac{\partial\delta\Psi}{\partial\theta}\right) = -\boldsymbol{\delta B}\cdot\nabla\Psi_0. \tag{1}$$

Dividing by $\boldsymbol{B}_0\cdot\nabla\varphi$ and Fourier transforming, we get

$$(n - \iota m)\delta\Psi_{\mathrm{nm}} = -\left(\frac{\boldsymbol{\delta B}\cdot\nabla\Psi_0}{\boldsymbol{B}_0\cdot\nabla\varphi}\right)_{\mathrm{nm}}. \tag{2}$$

The nonresonant Fourier components just introduce small ripples in the flux surfaces. If a resonant Fourier component is present (one satisfying $n = \iota m$), the flux surface is broken and a magnetic island is produced.

The response of a rotating plasma at the rational surface to an externally imposed resonant perturbation has been calculated theoretically for a variety of regimes and under a variety of assumptions [1, 18–23]. These calculations have been done for either slab or cylindrical geometry. Because the local induced current is determined by the layer physics, these calculations are relevant for shaped tokamaks and for stellarators.

The electromagnetic torque exerted on the rational surface by the resonant perturbation is opposed by a viscous torque produced by the plasma flow external to the surface. (In a nonaxisymetric configuration there is in general also a direct $\boldsymbol{j} \times \boldsymbol{B}$ torque exerted on the boundary layer at the rational surface by the nonambipolar radial current. This contribution to the torque is small for the cases we consider in this paper.) The threshold for resonant field penetration is determined by the relative magnitude of the electromagnetic torque and the viscous torque. While the physics determining the magnitude of the electromagnetic torque is the same in tokamaks and stellarators, the physics determining the viscous torque is modified in a stellarator by the radial current produced by the nonambipolar transport. In the absence of a resonant perturbation, this radial current produces an ambipolar potential and a corresponding contribution to the plasma flow. When a resonant perturbation is imposed, the electromagnetic torque causes the flow velocity to deviate locally from its ambipolar value. The radial current arising from the resulting nonambipolar transport produces a $\boldsymbol{j} \times \boldsymbol{B}$ torque that opposes the electromagnetic torque and enhances the effectiveness of the shielding.

Sections 3 and 4 discuss the calculation of the viscous torque for NCSX. Section 3 discusses the ambipolar plasma flow in the absence of a resonant magnetic perturbation. Section 4 discusses the viscous force that opposes the electromagnetic force produced by a resonant perturbation. Section 5 discusses the resulting penetration threshold for resonant magnetic perturbations.

3. Unperturbed ambipolar plasma flow in NCSX

In this section we calculate the plasma flow velocity profile in the absence of a resonant perturbation for our reference $\beta = 4\%$ NCSX equilibrium. We first calculate the ambipolar potential and corresponding flow neglecting the effect of radial momentum diffusion. We then bring in the effect of radial momentum diffusion (perpendicular viscosity) through the momentum diffusion equation. Determination of the appropriate boundary conditions for the momentum diffusion equation requires a consideration of momentum loss at the plasma boundary, and for this purpose we calculate the interaction with neutrals and with the Scrape-Off Layer (SOL). Our analysis does not include a momentum source term due to neutral beams. It is planned to heat NCSX with balanced beams so as to minimize the associated current drive in the plasma core.

3.1. Ambipolar potential and corresponding plasma flow neglecting radial momentum diffusion

We solve for the temperature profiles and self-consistent ambipolar potential using a model [7] which consists of a set of one-dimensional transport equations in cylindrical geometry, with an assumed density profile. The thermal diffusivities are calculated as the sum of three contributions: neoclassical ripple transport, neoclassical axisymmetric transport and an anomalous transport model with an adjustable coefficient. The neoclassical ripple transport is calculated from a single helicity analytical neoclassical ripple model [24–26] using an effective helical ripple obtained from the full three-dimensional numerical equilibrium. In particular, the calculation of the effective ripple in the $1/\nu$ regime uses a code developed by Nemov *et al* [27]. The neoclassical axisymmetric transport is given by the Chang–Hinton formulation for a circular plasma cross section [28], using the same cross sectional area as the toroidal average of NCSX, with a correction factor incorporated to give agreement with an axisymmetric NCLASS [29] calculation. Unlike many tokamaks, stellarators often have experimentally determined thermal diffusivities that are approximately radially constant, and we adopt this simple model for the anomalous transport, with the anomalous diffusivity adjusted to match a target thermal $\langle\beta\rangle$ or H factor.

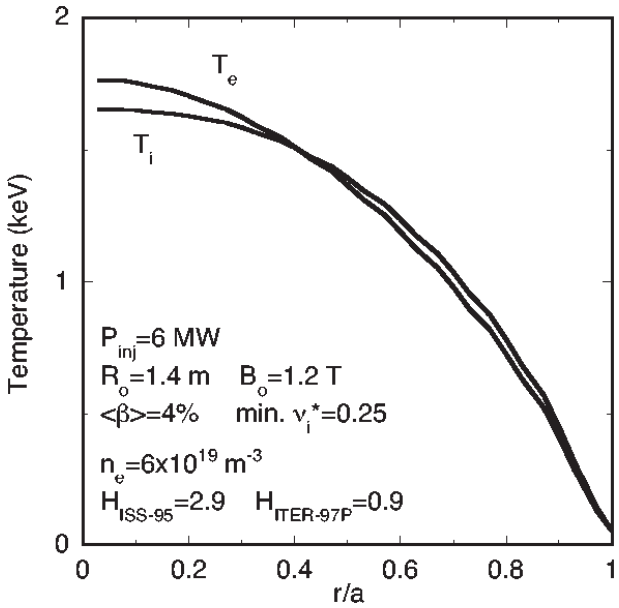

Figure 3. Calculated electron and ion temperature profiles for the reference NCSX equilibrium.

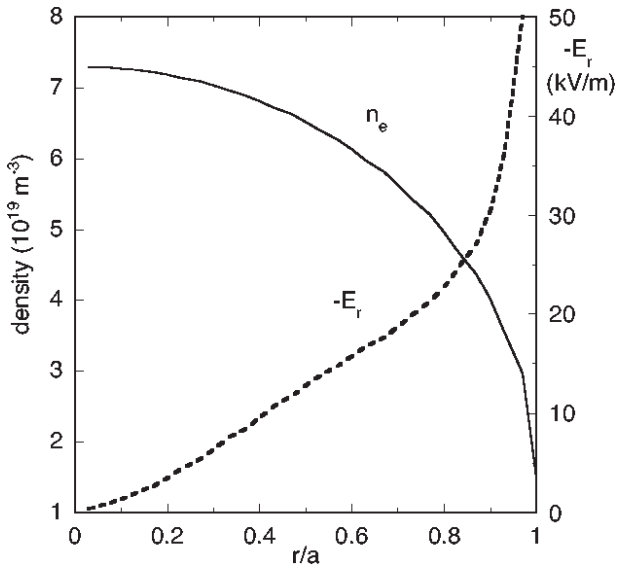

Figure 4. Electron density and ambipolar radial electric field for the reference NCSX equilibrium.

The transport model is described in more detail in [7]. The calculated electron and ion temperature profiles for our reference NCSX equilibrium are plotted in figure 3. The assume density profile is shown in figure 4. It is important to note that the thermal diffusivities are dominated by the contributions from anomalous and axisymmetric neoclassical transport, while only the helical neoclassical transport is expected to contribute to the nonambipolar radial transport. By varying the effective helical ripple it should be possible to change the radial currents while not significantly affecting the thermal diffusivities [7].

In the absence of a radial electric field, the ions are lost more rapidly than the electrons, giving a net outward current. The radial electric field, E_r, builds up until it is sufficiently large to equalize the radial flux of the ions and electrons, $j_\mathrm{r} = 0$. The calculated self-consistent ambipolar radial electric field is plotted in figure 4.

In steady state, the ion momentum equation determines the component of the flow perpendicular to the magnetic field: $v_{\mathrm{i}\perp} = \boldsymbol{E} \times \boldsymbol{B}/B^2 - (1/ne)\nabla p_\mathrm{i} \times \boldsymbol{B}/B^2$. There is in addition a component of the flow velocity aligned with the magnetic field, $v_\parallel$, and its magnitude is determined by the relative flow damping in the poloidal and toroidal directions. As in a tokamak, the damping in the poloidal direction is strong. The configuration is sufficiently close to quasi-axisymmetry that the flow damping in the toroidal direction is small. This implies that the flow velocity in the poloidal direction can be taken to be zero to a good approximation. In cylindrical geometry, we write $\boldsymbol{v} = v_\perp \hat{r} \times \hat{b} + v_\parallel \hat{b}$, where $\hat{b} = \boldsymbol{B}/B$, $\boldsymbol{B} = B_\mathrm{p}\hat{\theta} + B_\mathrm{t}\hat{\phi}$. Imposing the constraint $v_\theta = 0$, we get $v_\parallel = (B_\mathrm{t}/B_\mathrm{p})v_\perp$.

NCSX has a strong axisymmetric component of shaping, with an ellipticity of 1.8, and it has an aspect ratio of 4.3. We can ask what effect this geometry has on the calculation of the velocity driven by the ambipolar potential, whether there should be associated correction factors. This question can be approached by considering the geometric effects on an axisymmetric field. Starting from the usual mixed representation for an axisymmetric field, $\boldsymbol{B} = \nabla\psi \times \nabla\phi + F(\psi)\nabla\phi$, it is straightforward to obtain a corresponding expression for the perpendicular component of the velocity, and to determine the parallel component of the velocity from the condition that $v_\mathrm{p} = 0$. We find $|v_\perp|/|v_\phi| = |\nabla\psi|/F(\psi) = B_\mathrm{p}/B_\mathrm{t}$, and $v_\phi \approx R(\mathrm{d}\Phi/\mathrm{d}\psi - \mathrm{d}p_\mathrm{i}/\mathrm{d}\psi)$, where Φ is the ambipolar potential. It follows that our conclusions concerning the magnitude of the toroidal velocity are unaffected by the shaping.

Our calculation of v_ϕ depends on the fact that the deviation from quasi-axisymmetry is sufficiently small that the flow damping in the toroidal direction may be neglected relative to that in the poloidal direction. A criterion for the degree of quasi-axisymmetry required may be obtained by solving the momentum-balance equations in a flux surface [30, 31]. Working in Hamada coordinates, we write the ion flow as $v = v^\theta \boldsymbol{e}_\theta + v^\phi \boldsymbol{e}_\phi$, with $\boldsymbol{e}_{\theta,\phi}$ the contravariant basis vectors in the poloidal and toroidal directions. The steady-state parallel force balance equation is $0 = \langle \boldsymbol{B} \cdot \nabla \cdot \boldsymbol{\pi}_\mathrm{i} \rangle$, with $\boldsymbol{\pi}_\mathrm{i}$ the ion viscosity tensor. In the Pfirsch–Schlüter and plateau regimes, one has $\langle \boldsymbol{B} \cdot \nabla \cdot \boldsymbol{\pi}_\mathrm{i} \rangle \approx \mu_\theta v^\theta + \mu_\phi v^\phi$, and thus $v^\theta/v^\phi \approx \mu_\phi/\mu_\theta$. For a tokamak, axisymmetry implies $\mu_\phi = 0$, and thus $v^\theta = 0$. A criterion for our calculation of $\boldsymbol{e}_\phi \cdot \boldsymbol{v}$ for a quasi-axisymmetric stellarator to be valid is

$$1 \gg \frac{v^\theta}{v^\phi} = \frac{\mu_\phi}{\mu_\theta}. \tag{3}$$

In the Pfirsch–Schlüter regime, simple expressions for $\mu_{\theta,\phi}$ have been worked out [30] for model expressions for the magnetic field strength B. Taking a single helical component (m,n) with amplitude $B_0\delta$, one has $B = B_0[1 - \varepsilon\cos(\theta) - \delta\cos(m\theta + n\phi)]$, and

$$\mu_{\theta,\phi} = \frac{\mu_0 p_\mathrm{i}}{\nu_\mathrm{ii}} \left\langle \frac{\boldsymbol{B} \cdot \nabla B}{B} \frac{\partial_{\theta,\phi} B}{B} \right\rangle \approx \frac{\mu_0 p_\mathrm{i} B}{2\nu_\mathrm{ii}} (\iota m + n)(m,n)\delta^2.$$

Here, $\mu_0 = 4.095$, ν_ii is the ion–ion collision frequency, p_i is the ion pressure and $\iota \equiv q^{-1}$ is the rotational transform. Using

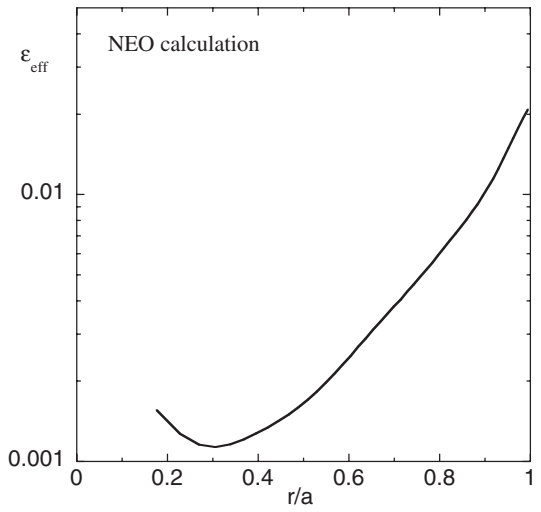

Figure 5. The effective helical ripple for NCSX versus the square root of the normalized toroidal flux as calculated by the NEO code.

this in equation (3) yields a ripple criterion for the validity of the analysis:

$$1 \gg \frac{(n/m)\Delta^2}{1+\Delta^2}, \tag{4}$$

where $\Delta^2 \equiv (m+nq)m\delta^2/\varepsilon^2$. Figure 5 is a plot of the effective helical ripple for the NCSX reference configuration. The dominant contributions to the ripple come from $m = 2, n = 1$, and from $m = 3, n = 2$. The ripple criterion, equation (4), is adequately satisfied.

3.2. Momentum diffusion and boundary conditions: interaction with neutrals and with the SOL

The calculation thus far has not taken into account momentum diffusion. We have taken the poloidal velocity to be zero because of the strong poloidal damping, and we only need to consider the toroidal component of the momentum diffusion equation. We consider the momentum diffusion equation in a cylinder, where it takes the form:

$$\rho \frac{\mathrm{d}v_z}{\mathrm{d}t} = \frac{1}{r}\frac{\mathrm{d}}{\mathrm{d}r}\left(\mu\rho r \frac{\mathrm{d}v_z}{\mathrm{d}r}\right) + j_r B_\theta. \tag{5}$$

Here ρ is the plasma density, v_z is the axial velocity, μ is the (anomalous) momentum diffusivity ($\mu\rho$ is the coefficient of perpendicular viscosity) and j_r is the current produced by nonambipolar radial transport. In tokamak experiments, the anomalous momentum diffusivity has been found to be approximately equal to the anomalous cross-field thermal diffusion coefficient, and we assume that that is also the case here. As mentioned above, stellarators often have experimentally determined thermal diffusivities that are approximately radially constant, and we adopt the simple model of taking μ to be radially constant. For our reference NCSX equilibrium, $\mu \approx 1.5\,\mathrm{m^2\,s^{-1}}$.

Equation (5) differs from the momentum diffusion equation in a tokamak by the presence of the last term, which is nonzero when the flow velocity on a flux surface is forced away from its ambipolar value.

Equation (5) must be supplemented by boundary conditions at the origin and at the edge. At the origin, regularity requires $\mathrm{d}v_z/\mathrm{d}r = 0$. At the plasma edge, the boundary condition is determined by the interaction with neutrals and with the SOL, which produce a momentum flow through the plasma edge equal to $-4\pi^2 aR\mu\rho\,\mathrm{d}v_z/\mathrm{d}r$, where a is the minor radius and R is the major radius. The momentum flow is equal to the total force exerted by the neutrals and SOL, which are taken to act on a radially narrow region at the plasma edge. (We will justify this approximation below.)

Near the plasma edge, momentum is transferred to the neutrals primarily through charge exchange. Ionization reactions also must be taken into account, because they serve to impart some of the momentum picked up by the neutrals back to the ions. To estimate the rate of momentum transfer to the neutrals we use the DEGAS code to do a Monte Carlo calculation for a model axisymmetric geometry [32]. We use the $\phi = \pi/6$ (bullet-shaped) cross section for this purpose, as is appropriate for the expected initial placement of a limiter on NCSX.

The momentum transfer to the neutrals is localized at the plasma edge, with the average momentum transfer rate in the zone $0.96 < r/a < 1$ calculated to be about seven times as large as that in the zone $0.92 < r/a < 0.96$. The rate of momentum transfer to the neutrals can be expected to scale roughly linearly with the plasma velocity. We write this momentum transfer rate as $\nu_n v_z$, where ν_n is a coefficient to be determined. For an edge velocity of $290\,\mathrm{km\,s^{-1}}$, the integrated momentum transfer rate is calculated to be about 1.2 N, corresponding to $\nu_n = 4\times10^{-6}\,\mathrm{kg\,s^{-1}}$. This gives the boundary condition $a\,\mathrm{d}v_z(a)/\mathrm{d}r = -\kappa v_z(a)$, with $\kappa \approx 2$.

We next estimate the momentum transfer to the SOL. We consider the case where there is a toroidal rail limiter. Field lines outside the plasma edge intercept the limiter, with a connection length of $L \approx \pi R/\iota$, where $\iota \approx 0.6$ is the rotational transform at the plasma edge. The ion mean free path is comparable to the connection length. Particles outside the plasma edge are lost to the limiter in a time $\tau \approx L/v_{\mathrm{ti}}$, so that the momentum loss rate in the SOL is approximately $\rho v_z/\tau$. Combining this with momentum diffusion, and adopting a slab approximation (which is appropriate in the narrow SOL), we get $(\mathrm{d}/\mathrm{d}r)[\mu\rho(\mathrm{d}v_z/\mathrm{d}r)] = \rho v_z/\tau$. The velocity decays exponentially as a function of r in the SOL, $v_z(r) = v_z(a)\exp(-(r-a)/l)$. The density obeys a similar equation, and it too decays exponentially in the SOL. If the diffusion coefficients are equal, $l \approx 1.6\sqrt{\mu\tau}$. Momentum is dissipated in the SOL at the rate $\int_a^\infty \rho v_z/\tau \approx 0.6\rho(a)v_z(a)\sqrt{\mu/\tau}$. The momentum transfer rate is again of the form $\nu_n v_z$, with the SOL contribution to ν_n estimated to be roughly $0.6\rho(a)\sqrt{\mu/\tau}$. The momentum transfer to the SOL is sensitive to the value of ρ at the edge. For our assumed density profile $n_{\mathrm{e}}(a) \approx 1.5\times10^{19}\,\mathrm{m^{-3}}$, and we calculate $\kappa \approx 18$. For smaller values of $n_{\mathrm{e}}(a)$, the momentum transfer to the SOL is correspondingly smaller, with the total momentum transfer rate bounded below by the contribution of the neutrals.

Having determined the boundary conditions, we return to the solution of equation (5). For this purpose, we must determine the dependence of j_r on v_z. The radial current vanishes when v_z has its ambipolar value, corresponding to the ambipolar value of the electrostatic potential. We adopt

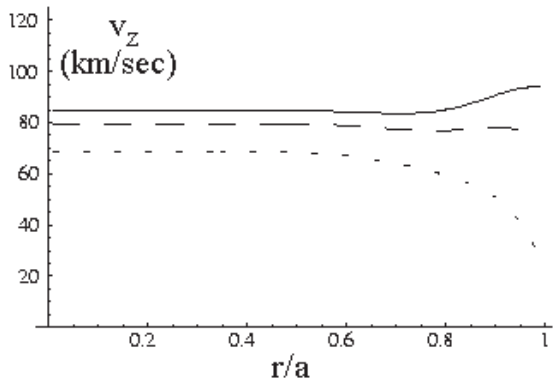

Figure 6. Calculated ambipolar velocity profiles for three different levels of momentum dissipation at the plasma edge. The three curves were obtained with $\kappa = 0$, $\kappa \approx 2$ and $\kappa \approx 18$, corresponding, respectively, to no momentum dissipation at the edge, to dissipation appropriate for neutral collisions only, and to dissipation produced by the SOL with $n_e(a) \approx 1.5 \times 10^{19}\,\mathrm{m}^{-3}$.

a simple linear approximation for j_r, interpolating between the values for $E_r = 0$ and for the ambipolar value of E_r. The last term in equation (5) can then be written in the form $j_r B_\theta \approx -\alpha(r)[v_z - v0(r)]$, where $v0$ is the ambipolar value of v_z (i.e. the value that v_z assumes when E_r has its ambipolar value). Equation (5) now assumes the linear form

$$\rho \frac{\mathrm{d}v_z}{\mathrm{d}t} = \frac{1}{r}\frac{\mathrm{d}}{\mathrm{d}r}\left(\mu\rho r \frac{\mathrm{d}v_z}{\mathrm{d}r}\right) - \alpha(r)[v_z - v0(r)] \qquad (6)$$

and can be solved numerically in a straightforward manner.

Figure 6 shows numerical solutions for the steady-state velocity profile for three different values of κ. The top curve corresponds to $\kappa = 0$, giving the velocity profile in the absence of momentum dissipation at the plasma edge. The middle curve was obtained with $\kappa \approx 2$, the lower bound on momentum dissipation due to collisions with neutrals. The bottom curve corresponds to $\kappa \approx 18$, the estimate for momentum dissipation in the SOL with the assumed value of $n_e(a)$. Because the ripple magnitude increases rapidly towards the plasma edge, the flow velocity profile is broad. As the q profile evolves during startup, low order rational surfaces entering from the plasma boundary are particularly vulnerable to resonant magnetic perturbations. The broad velocity profile in NCSX will provide relatively strong shielding for low order rational surfaces near the plasma edge, and this will potentially impact the options available for startup scenarios.

4. Viscous torque on rational surfaces

When a resonant magnetic field perturbation is imposed on a rotating plasma, the resulting electromagnetic force slows the plasma rotation at the rational surface. The electromagnetic force is balanced by a viscous force exerted by the neighbouring plasma on the rational surface, which opposes the slowing of the plasma at the rational surface. As the amplitude of the external perturbation is increased, the electromagnetic force increases, and the rotation velocity of the plasma at the rational surface decreases further. The magnitude of the viscous force on the rational surface is determined by the momentum diffusion equation.

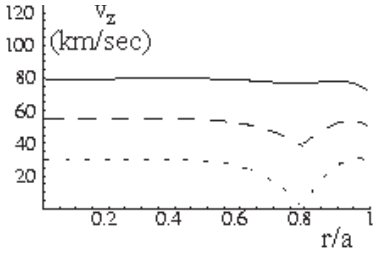

Figure 7. Numerical solution of the momentum diffusion equation for three different constraints at the rational surface, with $\kappa = 2$. The top curve (——) is the unconstrained solution. The middle and bottom curves correspond, respectively, to $v_s = v_{s0}/2$ and $v_s = 0$.

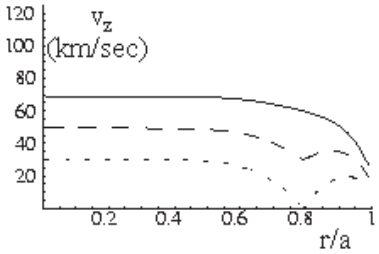

Figure 8. Numerical solution of the momentum diffusion equation for three different constraints at the rational surface, with $\kappa = 18$. Again, the top curve (——) is the unconstrained solution, while the middle and bottom curves correspond, respectively, to $v_s = v_{s0}/2$ and $v_s = 0$.

In addition to the viscous force on the rational surface, there is also a direct $\boldsymbol{j} \times \boldsymbol{B}$ torque exerted by the current that arises from the nonambipolar transport. The total torque exerted directly by the radial current is obtained by integrating the torque density across the boundary layer at the rational surface. For the case considered here, the viscous torque is estimated to be much larger than the torque exerted directly by j_r.

We again consider the reference NCSX equilibrium whose unperturbed velocity profile we discussed in the previous section. The $\iota = \frac{3}{5}$ rational surface is of particular concern because of its low order and because of its proximity to external perturbations. (It is located at $r/a \approx 0.8$.) The $m = 5$, $n = 3$ island proved to be the island that was the most difficult to suppress in the NCSX coil design process. We consider here the resonant mode penetration at the $\iota = 0.6$ rational surface in the presence of the ambipolar flow. Assuming that an externally generated $m = 5$, $n = 3$ perturbation slows the rotation of the rational surface, we calculate the countervailing viscous force. We solve the momentum diffusion equation for this purpose.

The steady-state solution of equation (6) is obtained under the assumption that the electromagnetic force has slowed the rotation to a fraction of its ambipolar value. Denote the velocity at the rational surface by v_s, and the unperturbed velocity at the rational surface by v_{s0}. We consider the case where $v_s = v_{s0}/2$, and the case where $v_s = 0$. Figures 7 and 8 show, respectively, the corresponding solutions of equation (6) for $\kappa \approx 2$ and $\kappa \approx 18$. In each plot, the top curve corresponds to the solution in the absence of an electromagnetic force, the middle curve corresponds to the solution when the velocity at the $\iota = 0.6$ rational surface is slowed to half its ambipolar value, and the

bottom curve corresponds to the solution when the rotation at the rational surface is entirely suppressed.

The viscous force exerted on the rational surface by the plasma flow is given by $4\pi^2 r R \rho \mu [\mathrm{d}v/\mathrm{d}r]^+_-$, where $[\mathrm{d}v/\mathrm{d}r]^+_-$ is the jump in the radial derivative of the fluid velocity across the associated boundary layer. For $\kappa \approx 2$, we calculate $a[\mathrm{d}v/\mathrm{d}r]^+_- \approx 274\,\mathrm{km\,s^{-1}}$ and $540\,\mathrm{km\,s^{-1}}$, respectively, for $v_s = v_{s0}/2$ and $v_s = 0$. For $\kappa \approx 18$ we calculate $a[\mathrm{d}v/\mathrm{d}r]^+_- \approx 238\,\mathrm{km\,s^{-1}}$ and $478\,\mathrm{km\,s^{-1}}$, respectively. Relative to v_0, the velocity on axis for the unconstrained velocity profile, we have $a[\mathrm{d}v/\mathrm{d}r]^+_- \approx 3.4 v_0$ and $6.8\ v_0$ for $\kappa \approx 2$, $a[\mathrm{d}v/\mathrm{d}r]^+_- \approx 3.5\ v_0$ and $7.0\ v_0$ for $\kappa \approx 18$.

We consider a simple model to compare the viscous force in a quasi-axisymmetric stellarator with that in a tokamak. Fitzpatrick [18] writes

$$\boldsymbol{v} = \boldsymbol{v}^{(0)} + \boldsymbol{v}^{(1)}, \tag{7}$$

where $\boldsymbol{v}^{(0)}$ is the velocity profile in the absence of the resonant perturbation, and he adopts the equation

$$\rho \frac{\mathrm{d}v_z^{(1)}}{\mathrm{d}t} = \frac{1}{r}\frac{\mathrm{d}}{\mathrm{d}r}\left(\mu\rho r \frac{\mathrm{d}v_z^{(1)}}{\mathrm{d}r}\right) \tag{8}$$

for the deviation of the toroidal velocity in a tokamak from its unperturbed value. This is valid as long as the plasma flow is driven by a momentum source which is independent of $\boldsymbol{v}$. If we substitute equation (7) into equation (6), we get

$$\rho \frac{\mathrm{d}v_z^{(1)}}{\mathrm{d}t} = \frac{1}{r}\frac{\mathrm{d}}{\mathrm{d}r}\left(\mu\rho r \frac{\mathrm{d}v_z^{(1)}}{\mathrm{d}r}\right) - \alpha v_z^{(1)}. \tag{9}$$

Relative to the tokamak, the stellarator has an additional term $-\alpha v_z^{(1)}$ on the right-hand side. To get some insight into the effect of this term, we consider the simple model where $\mu\rho$ and α are both assumed to be independent of r. The steady-state solutions of equation (9) are then the modified Bessel functions $I_0(\sqrt{\alpha/(\mu\rho)}r)$, $K_0(\sqrt{\alpha/(\mu\rho)}r)$. For $\alpha \gg \mu\rho$, these solutions have the asymptotic form $(\mu\rho/\alpha)^{1/4}\exp(\sqrt{\alpha/(\mu\rho)}r)/\sqrt{2\pi r}$ and $(\mu\rho/\alpha)^{1/4}\pi^{1/2}\exp(-\sqrt{\alpha/(\mu\rho)}r)/\sqrt{2r}$, so that the perturbed velocity profile has a gradient scale length of $(\mu\rho/\alpha)^{1/2}$. For $\alpha \to 0$, we recover the tokamak limit, where the scale length of the velocity gradient is comparable to r, so that the jump in $\mathrm{d}v/\mathrm{d}r$ is of the order of v/r. In a stellarator, the velocity gradient is affected by the magnitude of the nonambipolar $\boldsymbol{j} \times \boldsymbol{B}$ force, so that the gradient scale length can be shorter, imparting greater stiffness to the flow velocity, and enhancing the shielding effect.

5. Resonant mode penetration threshold

In mode penetration experiments on tokamaks where the amplitude of the external perturbation is gradually ramped up, it is found that the rational surface first slows to some fraction of its initial rotation frequency, and then abruptly ceases to rotate when the perturbation amplitude exceeds a threshold value. The cessation of rotation is accompanied by a complete penetration of the resonant perturbation at the rational surface. This is consistent with the predictions of theoretical calculations. The magnitudes of the viscous and electromagnetic forces are functions of v_s, and if $v_s > 0$ it must satisfy $F_{visc}(v_s) = F_{em}(v_s)$. There is predicted to be a threshold in the perturbation amplitude above which $F_{em}(v_s)$ exceeds $F_{visc}(v_s)$ for $0 \leqslant v_s \leqslant v_{s0}$, so that $v_s = 0$ when the perturbation amplitude exceeds this threshold.

The magnitude of F_{em} scales as the square of the resonant perturbation amplitude, with the functional dependence of $F_{em}(v_s)$ (i.e. the shape of $F_{em}(v_s)$) independent of the amplitude. Our numerical solution shows that $F_{visc}(v_s)$ is well approximated by a linear function of v_s, as it is in a tokamak, so that while its amplitude may be quite different, the functional dependence on v_s has not changed. It follows that there is again a threshold value of the resonant perturbation amplitude above which F_{em} dominates F_{visc}, and that at the threshold value v_s is the same as in the tokamak. The resonant mode penetration threshold scales as $F_{visc}^{1/2}$.

To estimate the magnitude of the flow-shielding effect for magnetic islands in NCSX, we compare with a resonant mode penetration experiment on DIII-D [4]. The DIII-D reference case has been chosen to have similar parameters to those in our NCSX reference equilibrium. It has $\langle\beta\rangle \approx 3.7\%$, $\langle n_e\rangle \approx 5 \times 10^{19}\mathrm{m}^{-3}$ and an ellipticity $\kappa \approx 1.8$. Our reference NCSX equilibrium has $\langle\beta\rangle = 4\%$, $\langle n_e\rangle = 6 \times 10^{19}\mathrm{m}^{-3}$ and an average axisymmetric component of ellipticity of 1.8. The magnetic field of both the DIII-D reference shot and the NCSX reference case is 1.2 T. The rotation frequency of the rational surface in the DIII-D reference shot is about 12 kHz. For the NCSX case, the predicted rotation frequency ranges from about 9 kHz for $\kappa \approx 2$ to about 7 kHz for $\kappa \approx 18$. DIII-D has $R \approx 1.67$ m and $R/\langle a\rangle \approx 2.1$, while NCSX has $R \approx 1.42$ m and $R/\langle a\rangle \approx 4.3$. The experimentally observed penetration threshold in the DIII-D reference case is $B_{r21}/B \approx 4 \times 10^{-4}$.

6. Discussion

The physics determining the penetration of a resonant magnetic perturbation in a stellarator differs from that in a tokamak due to the presence of a radial current produced by nonambipolar transport. As the electromagnetic force produced by the perturbation slows the rotation at the rational surface, the radial current driven by the resulting nonambipolar transport exerts a $\boldsymbol{j} \times \boldsymbol{B}$ force that resists departures from the ambipolar velocity and enhances the shielding effect. The unperturbed velocity profile is also modified in a stellarator. We have focused here on a particularly interesting regime, corresponding to an NCSX reference equilibrium, in which the configuration is sufficiently close to quasi-symmetry that the viscous damping in the toroidal direction is small, but the deviations from quasi-symmetry are sufficiently large to produce a substantial ambipolar flow, and a substantial modification of the flow-shielding effect. Because the ripple magnitude increases rapidly towards the plasma edge, the flow velocity profile is broad. The strong shielding for low order rational surfaces near the plasma edge will have potential implications for startup scenarios.

A reference DIII-D shot with parameters similar to those of our reference NCSX equilibrium has been reported to have a penetration threshold of $B_{r21}/B \approx 4 \times 10^{-4}$ [4]. Calculations with the PIES code found that the resonant $m = 5$, $n = 3$ field component associated with an initial NCSX coil design

algorithm that did not explicitly target resonant field error reduction was $B_{rnm}/B \approx 1.3 \times 10^{-3}$. This is likely above the penetration threshold, even including the enhancement of the shielding due to nonambipolarity, and a further coil optimization using the PIES code to reduce the magnitude of the resonant field components was a prudent step in the coil design process.

To the extent that the plasma flow shields out residual resonant magnetic field components at rational surfaces, it will further improve the flexibility of the NCSX device, and it will further reduce the vulnerability of the NCSX device to field errors.

The flexibility of the nonaxisymmetric NCSX device will potentially allow a variety of experiments to clarify the physics of the shielding of resonant magnetic perturbations by plasma flow. Control over the magnitude of the non-quasi-symmetric ripple will provide a knob for adjusting the magnitude of the nonambipolar current and the toroidal flow damping. Moreover, the thermal diffusivities are dominated by the contributions from anomalous and axisymmetric neoclassical transport, so they will not be significantly affected by modest changes of the effective helical ripple. The externally generated rotational transform will allow control over the q profile independent of the current profile. Simultaneous adjustment of the neutral beam power and the ohmic current drive will allow adjustment of the rotation frequency with a fixed current profile. Two sets of trim coils will provide control over the resonant components of the magnetic field. Comparison of the experiments with theoretical predictions will provide a new perspective on the physics of the shielding, and will contribute towards the goal of being able to reliably predict field-error penetration thresholds in tokamaks and stellarators.

Acknowledgment

This work was supported by DOE contract DE-AC02-76CH03073.

References

[1] Fitzpatrick R. and Hender T.C. 1991 *Phys. Fluids* B **3** 644
[2] Hender T.C. *et al* 1992 *Nucl. Fusion* **32** 2091
[3] LaHaye R.J. *et al* 1992 *Phys. Fluids* B **4** 2098
[4] LaHaye R.J. *et al* 1992 *Nucl. Fusion* **32** 2119
[5] Buttery R.J. *et al* 1999 *Nucl. Fusion* **39** 1827
[6] Nührenberg J., Lotz W. and Gori S. 1994 *Theory of Fusion Plasmas* ed E. Sindoni *et al* (Bologna: SIF)
[7] Mikkelsen D. *et al* Assessment of transport in NCSX *Fusion Sci. Technol.* submitted
[8] Reiman A. and Greenside H.S. 1986 *Comput. Phys. Commun.* **43** 157
[9] Reiman A. *et al* 2001 *Phys. Plasmas* **8** 3377
[10] Zarnstorff M.C. *et al* 2001 *Plasma Phys. Control. Fusion* **43** A237
[11] Neilson G.H. *et al* 2002 *Proc. 19th Int. Conf. on Fusion Energy (Lyon, 2002)* (Vienna: IAEA) CD-ROM file (IC-1) http://www.iaea.org/programmes/ripc/physics/fec2002/html/fec2002.htm
[12] Reiman A. *et al* Equilibrium and flux surface issues in the design of the National Compact stellarator experiment *Fusion Sci. Technol.* submitted
[13] Hudson S.R. *et al* 2002 *Phys. Rev. Lett.* 30, 2002
[14] Hudson S.R. 2002 *Plasma Phys. Control. Fusion* **44** 1377–82
[15] Hudson S.R. *et al* 2003 *Nucl. Fusion* **43** 1040
[16] Lazarus E.A. *et al* 2004 *Fusion Sci. Technol.* **46** 213
[17] Physics Design of NCSX *Fusion Sci. Technol.* special issue at press
[18] Fitzpatrick R. 1993 *Nucl. Fusion* **33** 1049
[19] Ma Z.W., Wang X. and Bhattacharjee A. 1996 *Phys. Plasmas* **3** 2427
[20] Wang X. and Bhattacharjee A. 1997 *Phys. Plasmas* **4** 748
[21] Hurricane O.A., Jensen T.H. and Hassam A.B. 1995 *Phys. Plasmas* **2** 1976
[22] Waelbroeck F.L. 2003 *Phys. Plasmas* **5** 4040
[23] Fitzpatrick R. 1998 *Phys. Plasmas* **5** 3325
[24] Shaing K.-C. 1984 *Phys. Fluids* **27** 1567
[25] Hastings D.E., Houlberg W.A. and Shaing K.-C. 1985 *Nucl. Fusion* **25** 445
[26] Crume E.C. Jr, Shaing K.C., Hirshman S.P. and van Rij W.I. 1988 *Phys. Fluids* **31** 11
[27] Nemov V.V. *et al* 1999 *Phys. Plasmas* **6** 4622
[28] Chang C.S. and Hinton F.L. 1986 *Phys. Fluids* **29** 3314
[29] Houlberg W.A., Shaing K.C., Hirshman S.P. and Zarnstorff M.C. 1997 *Phys. Plasmas* **4** 3230
[30] Coronado M. and Talmadge J.N. 1993 *Phys. Fluids* B **5** 1200
[31] Shaing K.C. and Callen J.D. 1983 *Phys. Fluids* **26** 3315
[32] Mioduszewski P. *et al* Power and particle handling and first wall in the National Compact Stellarator Experiment *Fusion Sci. Technol.* submitted